Confocal Imaging at 0.3 THz with Depth Resolution of a Painted Wood Artwork for the Identification of Buried Thin Metal Foils.

Chiara Ciano, Mariano Flammini, Valeria Giliberti, Paolo Calvani, Eugenio DelRe, Fabio Talarico, Mauro Torre, Mauro Missori and Michele Ortolani

***Abstract*— A compact confocal terahertz microscope working at 0.30 THz based on all-solid state components is used to locate buried thin metal foils in a painted wood artwork. Metal foils are used for decoration and their precise localization under the pictorial layer is relevant information for conservation scientists and restorers, which cannot be obtained neither by X-ray radiography nor by spectroscopic imaging in the infrared, as we directly show here. The confocal microscopy principle based on the spatial pinhole concept is here implemented by positioning the first focus of an ellipsoidal reflector at the phase center of horn antennas coupled to Schottky diode detector and emitter mounted in rectangular waveguide blocks, together with an optical beamsplitter. The second focus of the reflector is mechanically scanned inside the sample in three dimensions. The predictions of diffraction theory for a confocal microscope at an imaging wavelength of 1.00 mm with numerical aperture of 0.53 are verified experimentally (1.2 mm and 2.8 mm for the lateral and the axial resolution respectively). These values of resolution allow a precise determination of the position of buried metal foils in ancient piece of art hence making restoration interventions possible.**

***Index Terms*— Spatial resolution, high-resolution imaging, confocal microscopy, horn antennas, Schottky diode multiplier, Schottky diode detector, cultural heritage, diffraction limit.**

I. Introduction

IMAGING with sub-terahertz (THz) radiation [1] has a potential application in the non-destructive and non-invasive analysis of the internal structure of historical artworks [2-5]. The penetration depth of sub-THz radiation can be of several millimeters in dry organic matter (e.g. painting layers), a depth which is typically opaque to visible and infrared radiation. Therefore, THz imaging can be used to study the ground layers, the integrity of the substrate such as wooden panels or plaster layers [6], or the presence of buried crystal, glass or metal structures beneath the pictorial surface, which may participate to the final visual appearance of the artwork [7]. Due to the relatively high cost and complexity of THz components and systems [8], however, THz imaging can become popular among art historians and conservation scientists only if the information that it provides is impossible to obtain from other more common and/or more mature in-depth imaging techniques such as X-ray radiography, thermal imaging, and ultrasounds [7]. Portability of the imaging system is also a great advantage for cultural heritage studies, and from this point of view purposely engineered THz instruments can possibly outperform other techniques [8].

Terahertz time-domain spectroscopy (THz-TDS) was indeed shown to be suitable for cultural heritage studies [2, 7, 9-11] because it can be made portable and couples in-depth penetration with spectroscopic capabilities in a broad frequency range (usually 0.1 to 4 THz), where some pigments, crystal polymorphs and inks possess distinct vibrational spectroscopy features [2, 4]. The impressive development of portable X-ray radiation sources and related instrumentation for cultural heritage [12], however, has opened the way for in-situ elemental composition analysis by X-ray fluorescence spectroscopy (XRF), with very high sensitivity levels for traces of heavy elements. Organic matter, in turn, is typically analyzed by Raman spectroscopy and Fourier Transform Infrared (FTIR) spectroscopy, which are now featured by portable versions of the usual laboratory instruments [13]. Recently, "Terahertz Raman" spectrometers have been developed to access the same THz vibrational frequency range of THz-TDS, so as to distinguish polymorphs without directly employing any THz field [14]. Therefore, portable THz-TDS systems could complement more mature techniques for cultural heritage analysis mostly when in-depth imaging and spectroscopy are simultaneously required [15, 16]. In particular, THz-TDS excels when well-defined layered structures are present in the sample, because pulse-echo in-depth imaging techniques can be applied [17]. A clear

This work was supported in part by the Italian Ministry of Research through program SIR (Grant No. RBSI14IT0D).

C. Ciano, M. Flammini, P. Calvani, E. DelRe and M. Ortolani are with the Department of Physics, Sapienza University of Rome, Piazzale Aldo Moro 2, 00185 Rome, Italy (e-mail: chiara.ciano@uniroma1.it, mariano.flammini@uniroma1.it, eugenio.delre@uniroma1.it paolo.calvani@roma1.infn.it, michele.ortolani@roma1.infn.it).

V. Giliberti is with the Center for Life NanoSciences, Istituto Italiano di Tecnologia, Viale Regina Elena 291, 00161 Rome, Italy (e-mail: valeria.giliberti@iit.it).

M. Missori is with Institute for Complex Systems (ISC) of the National Research Council of Italy, Research Unit "Sapienza", Piazzale Aldo Moro 5, 00185 Rome, Italy (email: mauro.missori@isc.cnr.it)

M. Torre and F. Talarico are with Istituto Superiore per la Conservazione ed il Restauro, Via di San Michele 23, 00153 Rome, Italy (email: mauro.torre@beniculturali.it , fabio.talarico@beniculturali.it)

example is given by the study of ancient manuscripts. In Ref. 18, an array of written paper sheets acting as THz-transparent layered structures separated by air gaps, was investigated with time-gated techniques for three-dimensional content reconstruction [18]. Also, THz-TDS can be used to assess the conservation of paper supports through the hydrogen-bond network analysis of cellulose, as it probes the bulk of the paper sheet and not only its surface [19].

On the other end of the THz technology spectrum, a portable THz imaging system working at a single wavelength in continuous-wave mode is not yet commercially available [20-22]. Single-wavelength imaging allows for the introduction of advanced in-depth optical microscopy concepts taken from the visible range such as confocal imaging [23] and super-resolution imaging [24]. In confocal microscopy (CM), a full image of the sample can be obtained at different depth levels by using the spatial pinhole concept, which in the THz range can be implemented by employing microelectronic point emitters and detectors in a quasi-optical scheme [25]. According to Abbe's theory of diffraction and the subsequent developments of confocal laser microscopy theory [26], the confocal scheme with coherent illumination provides diffraction-limited lateral resolution given by:

$$\Delta x \approx \frac{0.82\,\lambda}{\sqrt{2}\,NA} \qquad (1)$$

where λ is the wavelength and NA is the numerical aperture of the focusing objective. The axial resolution is instead given by

$$\Delta z \approx \frac{4.4\,\lambda}{2\pi\,(NA)^2}\,. \qquad (2)$$

The numerical factors in (1) and (2) are obtained by numerical evaluation of the Airy function in the paraxial approximation, applying the half-width at half-maximum criterion [26]. At variance with the conventional formulas for the diffraction-limited resolution of standard microscopes, Eqs. (1) and (2) take into account that in confocal microscopy the focus is scanned inside the sample and the image is built one point at a time. Therefore, it is the focal spot size that determines the resolution. Note that, even if THz-TDS systems can also be used as confocal microscopes because they employ a point THz source and a point THz detector, their broadband spectrum implies that Eqs. (1) and (2) are undefined. In other words, the high lateral resolution seen in THz-TDS images is often carried by the high-frequency, short-wavelength component only.

In a single-wavelength quasi-optical scheme in the sub-THz range, large NA > 0.5 are possible [27]. This provides an opportunity for sub-millimeter resolution imaging with Schottky diode devices working at ν > 0.3 THz. If compared to other THz imaging techniques, sub-THz CM features depth resolution also in non-layered samples [20]. The reflector-to-sample distance can be kept around 10 mm, i.e., well above the sub-wavelength probe-to-sample distances typical of near-field imaging techniques [16, 28]. Moreover, sub-THz CM does not require physical contact unlike ultrasounds and

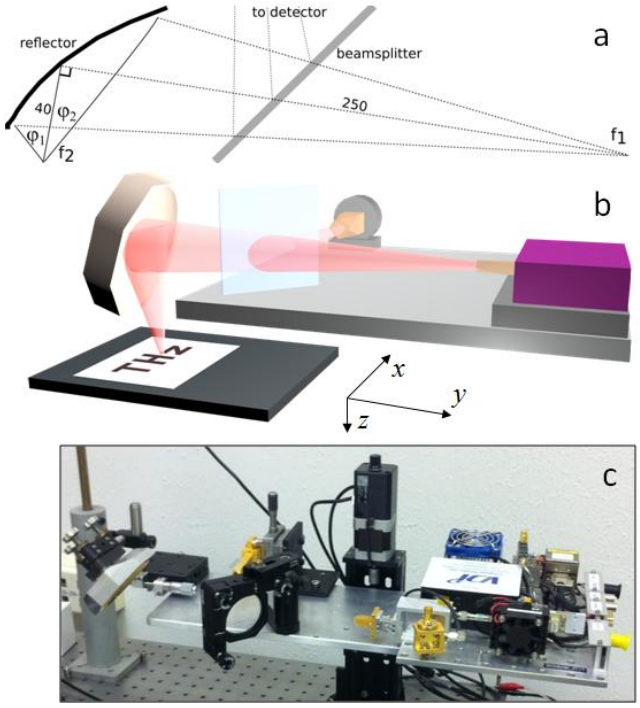

Fig. 1. Terahertz confocal microscope. (a) scheme of the 90° ellipsoidal reflector working as objective. The focal lengths are f_1 = 250 mm and f_2 = 40 mm and the angles of the objective side are φ_1=48° and φ_2=18°. (b) sketch of the microscope, with the sub-THz beam depicted in pink color. The letters "THz" represent the sample position and orientation. (c) Photograph of the sub-THz confocal microscope table with stepping motors.

magnetometers, and it can work in reflection mode unlike X-ray radiography. Also, X-ray imaging is difficult to achieve with portable X-ray sources, while a sub-THz CM system could be made portable by using all-solid state microelectronic components, as we do here [20, 21, 27].

In this paper we present a small-footprint sub-THz confocal microscope working at 0.30 THz (λ = 1.00 mm) and we use it to solve an art conservation problem that could not be solved with other methods. To attain small footprint, the microscope features a single focusing element and all-solid state emitter and detector, as sketched in Fig. 1a and 1band as shown in the photograph of Fig. 1c. We analyze the specific case of thin metal foils buried under painting layers in an ancient Russian wooden icon. We directly show that the precise shape of the metal foils is fully revealed by our sub-THz microscope while it could not be obtained by X-ray radiography, FTIR microspectroscopy or a near-infrared (NIR) camera. The experimental data will also allow us to verify the predictions of diffraction theory given in Eq. (1) and (2).

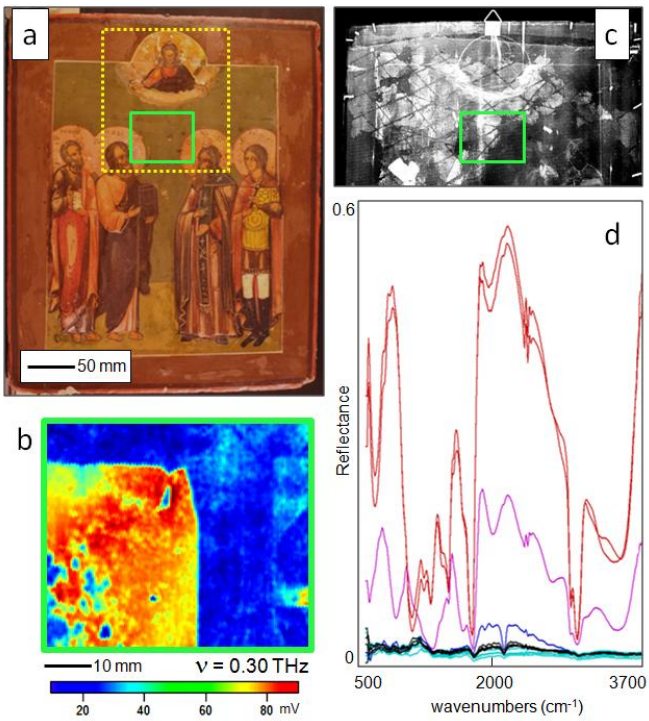

Fig. 2. Metal foil detection by high-resolution sub-THz CM and other techniques. (a) Photograph of the artwork. The green frame represents the area scanned in panel b, the yellow dotted frame the area scanned in Figures 3 and 4. (b) Sub-THz CM image of the area indicated by a green square in (a): the corner of a rectangular metal foil is clearly detected under the green painting layer. (c) X-ray radiograph of the upper half of the artwork. (d) MIR reflection spectra obtained by FTIR microspectroscopy at several positions along the left side of the green square. Red curves: lower locations with exposed metal foil (halo); light blue curves: upper locations outside the metal foil; black curves: intermediate locations with metal foil covered by painting layer.

II. Experiment

A. Microscope

We constructed the sub-THz CM system sketched in Fig. 1a which consists of an emitter, a detector, a beamsplitter and an ellipsoidal reflector. Confocal images are obtained either by a three-dimensional mechanical scan of the sample in the second reflector focus f_2 with a first stepping motors, or by a scan of the entire microscope table with a second set of stepping motors (Zaber Technolgies Inc., T-LSR series). An amplifier-multiplier chain (AMC by Virginia Diodes Inc.) followed by a cascade of rectangular waveguide-based Schottky diode multipliers (WR9.0 and WR2.8 triplers) coupled to a WR2.8 diagonal horn antenna is used as the sub-THz radiation source. The horn antenna transforms the rectangular waveguide mode TE_{10} into a free-space propagating Gaussian beam (TEM_{00}), linearly polarized along the vertical direction. The half-width at half-maximum beam divergence was estimated around 6° by the horn manufacturer. The center of an asymmetric ellipsoidal reflector at 90° angle (by Bruker Optics Inc., sketched in Fig. 1a) is positioned at 250 mm from the phase center of the horn antenna, i.e. with its first focus f_1 at the point emitter position. Being 50 mm the effective diameter of the reflector, the f/10 optics matched the beam divergence of the radiation source. The sample surface is positioned in proximity of f_2, at 40 mm from the reflector midpoint and at 12 mm from the physical edge of the reflector (see Fig. 1). Therefore, rough samples with asperities up to 11 mm (e.g. paintings with an extruded frame) can be safely scanned at high speed under the sub-THz CM. The detection arm consists of a 2 mm thick quartz beam-splitter, oriented at 45° with respect to the main beam axis, which directs the reflected beam into a second horn antenna coupled to a waveguide-block containing a zero-bias Schottky diode rectifier (WR2.8ZBD by Virginia Diodes Inc., with noise equivalent power 20 pW/Hz$^{0.5}$ and responsivity of 1500 V/W). The emitter is tuned at ν = 0.30 THz and the emitted power is approximately 1.0 mW. Considering a refractive index n = 2.11 for quartz at 0.30 THz, we calculate, for the first surface only (see Fig. 1a), a beam-splitter efficiency $(1\text{-}R)T^2R$ = 0.089 (where R = 0.138 and T = 0.861 are the single-interface power reflection/transmission coefficients). Electronic amplitude modulation at 10 kHz of the source intensity is employed together with a lock-in amplifier to retrieve the radiation intensity reflected by the sample. The lock-in output is sent to an analog-to-digital converter and then to a computer with a home-made MATLAB® routine that controls the stepping motors [20, 27]. When setting a 100 ms time window per pixel, including signal integration and dwell time for motor control, a signal-to-noise ratio of 10^3 is obtained. This value mainly results from fluctuations in intensity and frequency of the emitted radiation. A linescan along y with 5 pixels/mm over 10 cm then takes 50 s, and a total image of a 10 cm × 10 cm area with 2 lines/mm along x takes approximately 3 hours.

The implementation of the CM principle is obtained by positioning the first focus of the ellipsoid at the phase center of precisely manufactured horn antennas with efficient mode-to-mode conversion from the fundamental waveguide mode (TE_{10}) to the free-space fundamental Gaussian mode (TEM_{00}). The inverse conversion takes place in the detector's horn antenna [25]. This scheme also provides polarization selectivity, which concurs to reject scattered radiation and to increase the CM resolution [29]. The NA of the ellipsoidal reflector used as objective can be approximately calculated as the average of the sine of the two opening angles characterizing f_2: NA = $(\sin(\varphi_1)+\sin(\varphi_2))/2$ = 0.53. Direct measurement of the point-spread function of the microscope has validated this simple calculation [27]. Our microscope then is expected to provide a diffraction-limited lateral resolution $\Delta x \cong$ 1.1 mm according to (1) and an axial resolution $\Delta z \cong$ 2.8 mm according to (2), which are adequate values for the present sample under study.

B. Sample

The artwork under study is a Russian wooden icon of an unknown artisan dated back between the 17th and the 19th century. The icon is dedicated to the four saints of the Church: Apostles Peter and Paul, Cyril of Belozersk and George of Lydda lined up in the foreground and depicted in a three-quarter position. In the middle, above them, the Christ is

depicted, as a bust in the act of blessing with both hands rising from a cloud. (see Fig. 2a). The sample size is 32.5 cm height, 27.3 cm width, 2.5 cm thickness, which allowed for sample scanning under the microscope, however mechanical scan of the entire microscope table is also implemented for large-scale paintings that cannot be moved. Haloes of Christ and saints were obtained by the artist through application of a thin hammered metal foil (silver, thickness in the 0.1 to 0.5 μm range) on the ground layer; the foil was partially coated with translucent resin (colophony) to simulate the aspect of gold, while the remaining part of the silver foil was painted with organic pigments, also containing lead. The exact shape and position of the sharp edges of the metal foil constitutes essential information for the art conservation scientist, however they are not visible through the thick painting layer. X-ray radiography was performed in transmission mode on the entire icon with a digital medical apparatus (dose-area product of $7.4 \cdot 10^{-2}$ Gy·cm^2 with source peak voltage of 50 kV) but the metal foils did not appear in the radiographic image, because the absorption of a sub-μm thick metal foil is too low to be discernible in the X-ray imaging plate (see Table I). Moreover, the pigment contains lead, and the wood panel and ground layer are much thicker than the metal foils (pigment layer up to 1 mm, ground chalk layer up to a few mm). Since it is not possible in the available X-ray radiographs to distinguish between thin metal foils and other structures, this artwork represents a suitable case to demonstrate the application potential of sub-THz CM, which is instead expected to be very specific towards detection of metal surfaces.

III. Results

In Figure 2, the detection of metal foils under painted layers by the THz confocal microscope is summarized. The photograph in Fig. 2a shows the final visual effect of the shining halos of saints and the Christ, but it does not indicate the presence or the borders of the metal foils. The artist then covered the foils - apart from the circular areas forming the halos – and the bare wood around the foils with the same thick green painting layer. The artist could thus highlight the halos with the high visible-light reflectance of the unpainted metal foil areas. In Fig. 2b, it is shown the sub-THz CM image of the 60 mm × 50 mm area indicated by the green square in Fig. 2a: the precise borders of the metal foil are clearly seen as the boundaries of areas of the highest reflected power, corresponding to the foils, over a mostly non-reflecting background, corresponding to the wooden panel. The presence of the painted layers generates only minor features in the sub-THz CM image: indeed, the circular shape of the halo is barely visible in the bottom-left corner of Fig. 2b, characterized by low-reflectivity spots (blue color).

The X-ray radiographic image of the upper half of the artwork is shown in Fig. 2c: as anticipated, the metal foils are not detected due to their small absorption. A diagonal cross-hatch pattern of scratches, as well as other signs of the woodworking of the artist, have been identified in the X-ray radiograph. Calculations of the X-ray absorption of the different components of the artwork, reported in Table I, were performed in a simplified approach using the Beer-Lambert's law:

TABLE I
Calculation of X-ray absorption

Material	Thickness t	μ (cm^{-1})	Optical Density - log(I/I_0)
silver	0.1 μm	274.6	0.001
gold	0.1 μm	1010.9	0.004
aluminum	10 μm	6.14	0.003
wood1, dry	25 mm	0.23	0.249
wood2, wet	25 mm	0.24	0.260
colophony	100 μm	0.42	0.002
chalk	1 mm	19.23	0.835

Table I. X-ray absorption (in terms of optical density) of material layers as they are present in the investigated artwork. Thickness values t are just typical values encountered in the artwork. Gold and metallic aluminum foils are presumably not present, but displayed for reference in the table. The estimated weight fractions of elements are C 50%, O 43%, H 6% and N 1% for dry wood; and C 45.9%, O 46.8%, H 6.4% and N 0.9% for wet wood (9% moisture content). For the element fraction of colophony ad chalk, the chemical formulas $C_{20}H_{30}O_2$ and $CaSO_4$ were employed respectively. The X-ray linear attenuation coefficient for each element was obtained from [30]. Tabulated values were averaged between 16 keV and 41 keV X-ray photon energy.

$$I = I_0 e^{-\mu t} \qquad (3)$$

where I and I_0 are the incident and transmitted X-ray beam intensities respectively, μ is the X-ray linear attenuation coefficient and t is the thickness of the material. For elemental metals the absorption was calculated directly. The absorption coefficient of wood, colophony ($C_{20}H_{30}O_2$) and chalk ($CaSO_4$), instead, was obtained through a weighted average of the absorption coefficients of its constituent elements as:

$$\mu = \rho \sum_i w_i \left(\frac{\mu_i}{\rho_i}\right) \qquad (4)$$

where w_i are the weight fractions of elements (for wood i = 1, …, 4 for C, O, H, and N respectively, for colophony i = 1, …, 3 for C, O and H, and for chalk i = 1, ..., 3 for Ca, O and S), μ_i and ρ_i their absorption coefficient and partial densities, while ρ is a reference value for the wood density (for dry wood 0.49 g/cm^3, for wet wood 0.54 g/cm^3, for colophony 1.1 g/cm^3, and for chalk 2.5 g/cm^3). In Table I, the X-ray optical density OD = -log(I/I_0)=μt/2.303 for materials and thicknesses present in the artwork is reported. Thickness values t are just values typically encountered in this kind of artworks, as they obviously vary from point to point, and they were estimated from cross-sections of fragments of artworks of the same kind. One sees that the metal foils cannot be detected on the strong background from wooden panel and chalk layers, because it is very difficult to reliably detect an OD below 0.01 using X-ray imaging plates [31]. We note that it might have been possible to optimize the X-ray imaging contrast in a specific area to visualize the metal foils, but this would have required both knowledge of their presence and position in advance and additional X-ray scans.

In Fig. 2d, the mid-infrared (MIR) reflectance spectrum

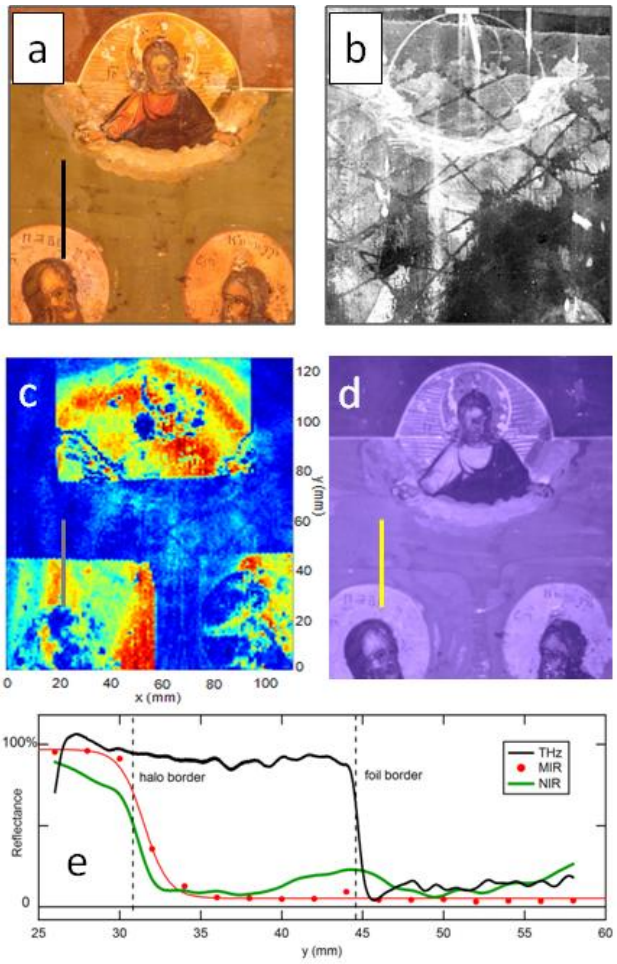

Fig. 3. (a) Photograph of the artwork area under analysis for metal foil detection (b) X-ray radiograph: the presence of metal foils cannot be detected (see Table I) . (c) Sub-THz CM: the three rectangular metal foils can be clearly imaged. (d) NIR imaging: foils not detected. (e) Comparison of line scans across one foil border taken with sub-THz CM (black curve), with FTIR microscopy in the MIR (red dots and red curve as a guide for the eye) and with NIR imaging (green solid curve). The sub-THz CM profile is taken from panel c at x = 18 mm, y scan from 25 to 58 mm (grey line in panel c). The MIR reflectance from Fig. 1d was integrated in the 1900-2300 cm^{-1} band of transparency of organic pigments. The NIR reflectance is extracted from the image data (yellow line in panel d corresponding to black line in panel a). The MIR and NIR data were normalized to their absolute value at y = 25 mm (R_{MIR} = 0.80 and R_{NIR} = 0.75, measured inside the halo by FTIR with respect to a gold mirror at λ = 5.0 μm and λ = 1.1 μm respectively).

taken at several positions across the metal foil border is shown in the 500 to 3700 cm^{-1} range, (or λ range 2.7 to 20 μm). The spectra are obtained by FTIR microspectroscopy with 100 μm × 100 μm aperture at 16 equidistant points along the left side of the sub-THz CM image in Fig. 2b parallel to the y axis. The red curves in Fig. 2d correspond to spectra taken at lower positions where the halo is visible to naked eye, the light blue curves correspond to positions outside the metal foil, and the black curves correspond to intermediate positions where the metal foil is present but covered by thick paint. The MIR vibrational fingerprints of pigments, glues and protective layers are clearly detected and will be discussed elsewhere. Concerning the detection of the metal foil, it can be seen that the black curves and the light-blue curves are almost identical, indicating that the MIR spectra do not add significant information to the observation in the visible, in terms of buried foil detection: a high MIR reflectance is obtained only when the halo is paint-free, at odds with sub-THz CM that almost ignores the presence of the painting layer. Only in a narrow frequency range between 1900 and 2500 cm^{-1} an imprint of the metal foil presence is seen as a very small difference between the MIR reflectance of locations outside the foil (black curves in Fig. 2d) and inside the painted foil (light blue curves). Finally, the dark blue curve in Fig. 2d shows a burst on the reflected intensity exactly at the border of the metal foil, where the painting layer thickness is possibly lower than far from the foil border. Clearly, the metal foils are much easily detected by sub-THz CM than by FTIR, while X-ray radiography just cannot detect them.

In Figure 3, the sub-THz CM image with the focal plane corresponding to the foil depth (Fig. 3c, same as center panel of Fig. 3) is directly compared with the corresponding areas of the photograph (Fig. 3a), with the X-ray radiographic image (Fig. 3b) and with the NIR image (Fig. 3d), the latter taken with a commercial camera sensitive to wavelengths between 0.7 and 1.1 μm (Nikon D90 Full Range). Clearly, only the sub-THz CM in Fig. 3b detects the metal foils, providing their position and dimensions with high resolution.

In Figure 3e, a sub-THz CM linescan is compared to the NIR and MIR reflectance values measured along the same line. The X-ray linescan has not been reported in Figure 3e as it would bear information on the wooden substrate and on the painting layers only, not on the metal foils. The sub-THz CM linescan (black solid line) is a profile extracted from the image data in Fig. 3c at x = 18 mm, with y varying from 58 to 25 mm with oversampled steps of 0.1 mm: a clear step is seen at the foil border for y = 44 mm. The NIR linescan (green solid line) detects only the halo border at y = 25 mm, also seen in the visible photograph, while the buried metal foil is detectable as a broad local maximum between y ~ 42 mm and y ~ 46 mm hence with much lower precision than for the sub-THz CM image. The absolute MIR reflectance R_{MIR} was measured by FTIR at equidistant locations (x = 18 mm, $26 \le y_i \le 56$ mm, i = 0, .., 15 and y_{i+1}-y_i = 2 mm). Inside the halo, the maximum value R_{MIR} = 0.80 is reached. The MIR reflectance was then integrated in the 1900 to 2300 cm^{-1} range, where the absence of vibrational fingerprints of organic matter around λ = 5 μm makes the painted layer partly transparent. Also the MIR reflectance displays a clear step at the halo border at y ~ 25 mm and a very weak local maximum at the foil border position (y = 44 mm). We can interpret the local maxima of NIR and MIR reflectances in Fig. 3e around y ~ 44 mm as the position of minimum thickness of the painting layer. The contrast and the positioning precision provided by sub-THz CM at the metal foil border, however, is by far greater than that provided by MIR and NIR imaging.

From the plot of Fig. 3e one can also precisely evaluate the lateral resolution Δy from the sub-THz CM linescan (black solid line). We estimate Δy ~ 0.9 mm from the 10%-90% profile value criterion [32]. If one assumes a typical value for

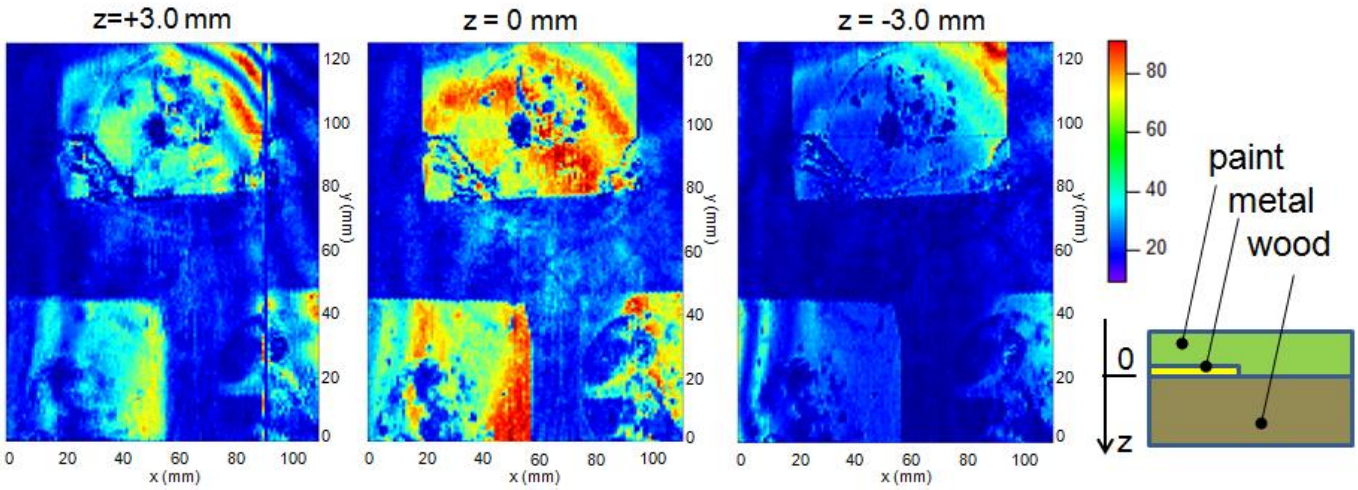

Fig. 4. Confocal imaging with depth resolution of the central area (110 mm × 125 mm) of the artwork at ν = 0.30 THz. Three rectangular metal foils are clearly detected. The z = 0 position is the one that gives best contrast for the rectangular metal foils, therefore it corresponds to the condition where the image object plane intercepts most of the metal foil surface. The image at z = + 3 mm has the object plane inside the sample, while the image at z = - 3 mm has the object plane close to the sample surface. The color scale is the sub-THz reflected intensity detected by the Schottky diode detector, in percentage of the lock-in amplifier full scale of 100 mV.

the refractive index of organic painting layers at 0.300 THz around $n \cong 1.3$ [2] hence a wavelength in the dielectric medium of $\lambda_d = \lambda/n \cong 0.77$ mm, the observed value Δy corresponds well with the prediction of Eq. (1) for the diffraction-limited lateral resolution. To summarize, THz confocal microscopy can clearly detect with millimeter resolution metal foils buried under painting layers, which are elusive for X-ray radiography, NIR imaging, and FTIR microspectroscopy in the MIR.

In Figure 4, three sub-THz CM images with depth resolution are shown for different values of z. Once the optimal working distance for optimizing the contrast between the metal foil and the background was found and set as z = 0, the sub-THz CM image of an enlarged area (110 mm × 125 mm, corresponding to the yellow dotted frame in Fig. 2a) has been taken. As shown in Fig. 3, sub-THz CM unveils three distinct rectangular metal foils. The different contrast measured at different positions for the three foils suggests that both the distance of the foils from the painted surface and the orientation of the foil surface normal vary with x, y, as expected because the surface of the wooden panel is not perfectly flat. Also, circular fringes are seen in the top-right corner of the image at z = 0, extending both inside and outside the metal foil area, possibly due to Fabry-Perot interference in the painting layer. Beyond such minor effects, the dimension, position and borders of the three rectangular foils are clearly imaged by sub-THz CM at the optimal contrast distance z = 0: one foil for the halos of the two characters on the left of the scene, one for the halos of the two characters on the right, and one for the Christ bust on top of the painting.

Afterwards, the microscope table (including the reflector and all optics, see Fig. 1b) was first raised and then lowered by 3.0 mm, a value slightly larger than the expected axial resolution Δz, and two sub-THz CM images were acquired by scanning the sample in x, y, reported as left and right panels in Fig. 4. The three images at z = 0, ±3.0 mm display very different contrast for the three foils, although the foils can still be detected in all images. The image at z = +3.0 mm (left panel of Fig. 4) displays high contrast only for the foil areas closer to the surface, while those far from the focal plane display almost no contrast. The image at z = -3.0 mm with the focal plane deep into the wood bulk (right panel of Fig. 4) displays almost no contrast between foils and support, apart from a foil area in the top-right corner, which may be buried more deeply below the painted surface. The weak imprint of the foils in the image at z = -3.0 mm (light blue rectangular areas in the right panel of Fig. 4) is to be attributed to residual scattering from out-of-focus foil areas, which are now crossed by the sub-THz beam before it reaches the focal plane. Interestingly, a cross-hatch pattern appears in the middle of the center and right panels of Fig. 4, but it is absent in the left panel. This cross-hatch pattern is very clearly seen in the X-ray image of Fig. 2c and 3b, and it is attributed to scratches intentionally dug into the wooden panel by the artist, probably in order to remove a previously painted scene. In fact, the scratches are not detected in the image taken at z = +3.0 mm hence confirming that the images are truly confocal and that attenuation and scattering from e.g. wood can be safely neglected at 0.30 THz [33]. The clear difference in the three images of Figure 4 also suggests that an axial resolution $\Delta z \sim$ 3 mm may be reached by our microscope, as expected from Eq. (2).

We now briefly discuss the performance of our sub-THz CM system if compared to those expected from a commercial pulsed THz-TDS imager with a broadband spectrum. As noted in previous comparison studies [34], exploiting pulse-echo techniques the depth resolution of THz-TDS pulsed system can be increased beyond the diffraction-limited confocal resolution achievable with a CW far-field system: in Ref. 18, a depth resolution of 0.3 mm with a THz-TDS technique using broadband pulses with wavelengths ranging from 3 to 0.3 mm, while the sophisticated CW imaging system of Ref. 35,

employing λ = 0.56 mm, could not attain Δz < 3 mm, well with the estimated depth resolution of our sub-THz CM employing λ = 1.00 mm. More stringent tests of the actual axial resolution of the present system on step-like metal structures are ongoing.

IV. Conclusions

A portable quasi-optical sub-terahertz confocal microscope was constructed to test the applicability of single-wavelength imaging with depth resolution to the study of cultural heritage and to its conservation. A painted wood artwork containing metal foils buried under painting layers was imaged with the microscope operating at 0.30 THz. The expected diffraction-limited lateral resolution of 1.1 mm was verified by imaging the borders of the buried metal foils. The estimate of the confocal axial resolution of 2.8 mm was approximately verified by displacing the focal plane by 3 mm above and below the metal foil plane and obtaining distinct contrast values. Detection of the position and size of the same metal foils was not possible with standard X-ray radiography, and it was only roughly achieved by near-infrared imaging or Fourier-transform infrared microspectroscopy, indicating that high-resolution terahertz imaging with depth resolution offers novel and unique opportunities to the study and the conservation of cultural heritage.

Acknowledgment

A sincere thanks to the iconologist Dr. Pietro Beresh (Department of the Arts of the Vatican Museums) for his kindness to study the icon and to provide valuable historical and stylistic information.

References

[1] W. L. Chan, J. Deibel, and D. M. Mittleman, “Imaging with terahertz radiation,” *Rep. Prog. Phys.* vol. 70, pp. 1325–1379, 2007.

[2] J. B. Jackson, J. Bowen, G. Walker, J. Labaune, G. Mourou, M. Menu, and K. Fukunaga “A Survey of Terahertz Applications in Cultural Heritage Conservation Science” *IEEE Trans. on Terahz. Sci. Technol.*, vol. 1, pp. 220-231, 2011.

[3] G. P. Gallerano, K. Fukunaga, and M. Picollo “Guest Editorial: Special Issue on THz Radiation Applied to Cultural Heritage” *J. Infrared Milli. Terahz. Waves*, vol. 38, n. 4, pp. 367–368, Apr. 2017.

[4] T. Bardon, R. K. May, P. F. Taday, and M. Strlic, “Systematic study of terahertz time-domain spectra of historically informed black inks” *Analyst* vol. 138, pp. 4859-4869, 2013.

[5] C. L. Koch Dandolo, A. Cosentino, and P. Uhd Jepsen, “Inspection of panel paintings beneath gilded finishes using terahertz time-domain imaging” *Studies in Conservation* vol. 60, n. 1, pp. S159-S166, 2015.

[6] J. B. Jackson, M. Mourou, J. F. Whitaker, I. N. Duling III, S. L. Williamson, M. Menu, and G. A. Mourou, “Terahertz imaging for non-destructive evaluation of mural paintings,” *Opt. Commun.* vol. 281, pp. 527–532, 2008.

[7] C. L. Koch Dandolo, K. Fukunaga, Y. Kohzuma, K. Kiriyama, K. Matsuda, and P. U. Jepsen, "Inspection of Asian Lacquer Substructures by Terahertz Time-Domain Imaging (THz-TDI)" *J. Infrared Milli. Terahz. Waves*, vol. 38, n. 4, pp. 425–434, Apr. 2017.

[8] S. S. Dhillon et al., “The 2017 terahertz science and technology roadmap” *J. of Phys. D: Appl. Phys.* vol. 50, n. 4, 043001, 2017.

[9] E. Abraham, A. Younus, A. El Fatimy, J.C. Delagnes, E. Nguéma and P. Mounaix, “Broadband terahertz imaging of documents written with lead pencils”, *Opt. Commun.* vol. 282, pp. 3104–3107, 2009.

[10] K. Krügener, M. Schwerdtfeger, S. F. Busch, A. Soltani, E. Castro-Camus, M. Koch and W. Viöl, "Terahertz meets sculptural and architectural art: Evaluation and conservation of stone objects with T-ray technology, *Sci. Rep.* vol. 5, p. 14842, 2015.

[11] K. Fukunaga, “THz Technology Applied to Cultural Heritage in Practice”, Springer, Berlin 2016.

[12] F. P. Romano, C. Caliri, P. Nicotra, S. Dimartino, L. Pappalardo, F. Rizzo, and H. C. Santos, “Real-time elemental imaging of large dimension paintings with a novel mobile macro X-Ray Fluorescence (MA-XRF) scanning technique.” *J. Anal. Atomic Spectrom.* vol. 32, n. 4, 2017.

[13] Agilent application note n. 5991-6976EN, Nov. 2016 http://www.agilent.com/en/products/ftir/ftir-compact-portable-systems/4300-handheld-ftir

[14] S. Lebedkin, C. Blum, N. Stürzl, F. Hennrich, and M. M. Kappes "A low-wavenumber-extended confocal Raman microscope with very high laser excitation line discrimination” *Rev. Sci. Instr.* vol. 82, p. 013705, 2011.

[15] D. van Mechelen, A.B. Kuzmenko, and H. Merbold "Stratified dispersive model for material characterization using terahertz time-domain spectroscopy”. *Optics Letters* vol. 39, n. 13, pp. 3853-3856, July 2014.

[16] O. Mitrofanov, M. Lee, J. W. P. Hsu, I. Brener,R. Harel, J. F. Federici, J. D. Wynn, L. N. Pfeiffer and K. W. West, "Collection-Mode Near-Field Imaging With 0.5-THz Pulses", *IEEE J. Sel. Top. Quant.* vol. 70, pp. 600-607, 2001.

[17] T. Buma and T. B. Norris, “Time reversal three-dimensional imaging using single-cycle terahertz pulses,” *Appl. Phys. Lett.* vol. 84, n. 12, pp. 2196–2198, 2004.

[18] A. Redo-Sanchez, B. Heshmat, A. Aghasi, S. Naqvi, M. Zhang, J. Romberg, and R. Raskar "Terahertz time-gated spectral imaging for content extraction through layered structures", *Nat. Commun.* 7, p. 12665, 2016.

[19] M. Peccianti, R. Fastampa, A. Mosca Conte, O. Pulci, C. Violante, J. Łojewska, M. Clerici, R. Morandotti, and M. Missori “Terahertz Absorption by Cellulose: Application to Ancient Paper Artifacts”, *Phys. Rev. Appl.* 7, 064019, 2017.

[20] M. Flammini, C. Bonsi, C. Ciano, V. Giliberti, E. Pontecorvo, P. Italia, E. DelRe, and M. Ortolani "Confocal Terahertz Imaging of Ancient Manuscripts" *J Infrared Milli Terahz Waves* vol. 38, n. 4, pp 435–442, Apr. 2017.

[21] N. Karpowicz, H. Zhong, C. Zhang, K.-I. Lin, J.-S. Hwang, J. Xu, and X.-C. Zhang, “Compact continuous-wave subterahertz system for inspection applications,” *Appl. Phys. Lett.* vol. 86, p. 054105, 2005.

[22] R. Wilk, F. Breitfeld, M. Mikulics, and M. Koch, “A continuous wave THz spectrometer as a noncontact thickness measuring device,” *Appl. Opt.* vol. 47, n. 16, pp. 3023–3026, 2008.

[23] M. A. Salhi, I. Pupeza, and M. Koch “Confocal THz Laser Microscope” *J Infrared Milli Terahz Waves*, vol. 31, pp. 358–366, 2010.

[24] M. Flammini, E. Pontecorvo, V. Giliberti, and M. Ortolani “Evanescent-Wave Filtering in Images Using Remote Terahertz Structured Illumination” *Phys. Rev. Applied*, vol. 8, p. 054019, 2017.

[25] A. Kazemipour, M. Hudlicka, R. Dickhoff, M. Salhi, T. Kleine-Ostmann and T. Schrader, “The Horn Antenna as Gaussian-Source in the mm-Wave Domain” *J. Infra. Milli. Terahz. Waves* vol. 35, pp. 720–731, 2014.

[26] C.-B. Juang, L. Finzi, and C. J. Bustamante, “Design and application of a computer-controlled confocal scanning differential polarization microscope,” *Rev. Sci. Instrum.* vol. 59, n. 11, pp. 2399–2408, 1988.

[27] V. Giliberti, M. Flammini, C. Ciano, E. Pontecorvo, E. DelRe, and M. Ortolani "Super-Resolved Terahertz Microscopy by Knife-edge Scan", *Proc. SPIE* vol. 10383 “Terahertz Emitters, Receivers, and Applications VIII”, p. 103830 (2017/08/23).

[28] A. Doria, E. Giovenale, G. P. Gallerano, M. Picollo, and K. Fukunaga, "A millimeter wave/terahertz 3D scanner for wall painting investigation" *Infrared, Millimeter, and Terahertz waves (IRMMW-THz), 2014 39th International Conference on*

[29] N. van der Valk, W. A. M. van der Marel, and P. C. M. Planken, “Terahertz polarization imaging,” *Opt. Lett.* vol. 30, n. 20, pp. 2082–2084, 2005.

[30] https://www.nist.gov/pml/x-ray-mass-attenuation-coefficients.

[31] R. D. Jayasinghe, B. S. Weerakoon and R. Perera "Evaluation of development time effect on X-ray film density", *Int. J. Mod. Alt. Med. Res.* Vol. 3, pp. 1-4, 2015.

[32] T. Löffler, T. Bauer, K. J. Siebert, H. G. Roskos, A. Fitzgerald, and S. Czasch, "Terahertz dark-field imaging of biomedical tissue," *Opt. Express* vol. 9, n. 12, pp. 616–621, 2001.
[33] M. Reid and R. Fedosejevs, "Terahertz birefringence and attenuation properties of wood and paper", *Appl. Optics* vol. 45, p. 2770, 2006.
[34] N. Karpowicz, H. Zhong, J. Xu, K.-I. Lin, J.-S. Hwang and X.-C. Zhang, "Comparison between pulsed terahertz time-domain imaging and continuous wave terahertz imaging" *Semiconductor Science and Technology*, vol. 20, n. 7, S293, 2005.
[35] N. Sunaguchi, Y. Sasaki, N. Maikusa, M. Kawai, T. Yuasa, C. Otani, "Depth-resolving THz imaging with tomosynthesis", *Opt. Express*, vol. 17, pp. 9558-9570, 2009.

Mauro Missori received the Italian Laurea degree in Physics in 1990 and the Ph.D. degree in Physics in 1994, both from Sapienza University of Rome. He also received a Ph.D. degree in Biophysics from the Università Cattolica Sacro Cuore, Rome, Italy, in 2010. From 2001 to 2009 he was Scientific Officer in Physics with the Italian Ministry of Cultural Heritage.

He is currently a Researcher with the Institute of Complex Systems (ISC) of the National Research Council of Italy. He also leads the ISC Cultural Heritage Applied Spectroscopy Laboratory, where he is involved in the development of advanced diagnostic systems for ancient artworks. His research interests include THz spectroscopy of biopolymers and optics of disordered media.

In 2016, he received the Special Mention for Communications within the Applied Physics section at the 101st Annual Congress of the Italian Physical Society.

Valeria Giliberti was born in 1987. She conducted her PhD research at the Institute for Photonics and Nanotechnologies (IFN) of the National Research Council of Italy (2011-2014), and continued to postdoctoral studies at Sapienza University of Rome where she was part of official staff of the European project GEMINI (2014-2016).

Since April 2016, she is postdoctoral fellow at the at the Center for Life NanoScience IIT@Sapienza of Istituto Italiano di Tecnologia (IIT), working on the design, construction and implementation of infrared and terahertz imaging systems, including near-field imaging.

Michele Ortolani was born in 1977 in Rome (Italy). He conducted his PhD research on terahertz spectroscopy of superconductors at Sapienza University of Rome (2005), and continued to postdoctoral studies at the BESSY Synchrotron Radiation facility of the Helmoltz Zentrum Berlin, Germany (2006-2007). In 2008-2010, he was coordinator of a national project on Terahertz imaging at the Institute for Photonics and Nanotechnology (IFN) of the National Research Council of Italy.

Since 2011, he is Assistant Professor at the Department of Physics of Sapienza University of Rome. His research topics include the study and fabrication of terahertz antennas on semiconductor materials, the development of silicon-germanium heterostructures towards a silicon-based terahertz quantum cascade lasers, and the application of advanced laser microscopy and imaging concepts to the terahertz range.

Dr. Ortolani was a member of the Local Organizing Committee of the IEEE Conference on Infrared, Millimeter and Terahertz Waves (IRMMW-THz) hold in Rome in 2010, and of the International Advisory Committee in 2012, 2014, and 2016 editions of the same Conference.